JACS
JOURNAL OF THE AMERICAN CHEMICAL SOCIETY

Article

pubs.acs.org/JACS

Activation of White Phosphorus by Low-Valent Group 5 Complexes: Formation and Reactivity of *cyclo*-P_4 Inverted Sandwich Compounds

Clément Camp,[†] Laurent Maron,*[,‡] Robert G. Bergman,*[,†] and John Arnold*[,†]

[†]Department of Chemistry, University of California, Berkeley, California 94720, United States

[‡]LPCNO, INSA Toulouse, Université de Toulouse, 135 Avenue de Rangueil, 31077 Toulouse, France

Supporting Information

ABSTRACT: We report the synthesis and comprehensive study of the electronic structure of a unique series of dinuclear group 5 *cyclo*-tetraphosphide inverted sandwich complexes. White phosphorus (P_4) reacts with niobium(III) and tantalum(III) β-diketiminate (BDI) *tert*-butylimido complexes to produce the bridging *cyclo*-P_4 phosphide species $\{[(BDI)(N^tBu)M]_2(\mu\text{-}\eta^3{:}\eta^3P_4)\}$ (**1**, M = Nb; **2**, M = Ta) in fair yields. **1** is alternatively synthesized upon hydrogenolysis of $(BDI)Nb(N^tBu)Me_2$ in the presence of P_4. The trinuclear side product $\{[(BDI)NbN^tBu]_3(\mu\text{-}P_{12})\}$ (**3**) is also identified. Protonation of **1** with $[HOEt_2][B(C_6F_5)_4]$ does not occur at the phosphide ring but rather involves the BDI ligand to yield $\{[(BDI^{\#})Nb(N^tBu)]_2(\mu\text{-}\eta^3{:}\eta^3P_4)\}[B(C_6F_5)_4]_2$ (**4**). The monocation and dication analogues $\{[(BDI)(N^tBu)Nb]_2(\mu\text{-}\eta^3{:}\eta^3P_4)\}\{B(Ar^F)_4\}_n$ (**5**, n = 1; **6**, n = 2) are both synthesized by oxidation of **1** with $AgBAr^F$. DFT calculations were used in combination with EPR and UV−visible spectroscopies to probe the nature of the metal−phosphorus bonding.

INTRODUCTION

Since its discovery in the middle of the 17th century, elemental phosphorus has fascinated chemists. Even still, novel allotropes of this element continue to be discovered and studied.[1] Among these, white phosphorus (P_4) is readily available as the direct product of reduction of phosphate minerals[2] and could be used directly as a building block for synthesizing a wide array of phosphorus-containing inorganic and organic products. Currently, most industrial processes involve molecular phosphorus chlorination or oxychlorination to PCl_n and $POCl_3$ before derivatization.[3,4] The development of environmentally friendly and atom-efficient strategies for the direct functionalization of P_4 to organo-phosphorus products, polyphosphorus cages, and other P-containing inorganic derivatives is therefore highly desirable.

A classic methodology for activating white phosphorus involves using well-identified or in situ generated reduced metal complexes.[5−17] Depending on the reducing ability, nature, and coordination environment, a wide array of metal−phosphide species can be generated.[3,4,18−20] Despite several recent achievements in the subsequent transformation of these activated metal−phosphorus species,[7,21−28] direct incorporation of P atoms from P_4 under mild conditions both stoichiometrically and catalytically remains a great challenge for contemporary main group and transition metal organometallic chemists. This notably requires a deeper understanding of the nature of the metal−phosphide interaction and the reaction processes involved.

To date, the formation of square-planar *cyclo*-tetraphosphide species from P_4 has only been observed on rare occasions.[8,29−33] Examples of compounds containing a *cyclo*-tetraphosphide motif bridging two metal ions in a symmetrical fashion, also known as *cyclo*-P_4 inverted sandwiches, remain extremely limited, and their chemical properties are almost unexplored. Reported examples of bimetallic inverted sandwiches are neutral and of general formula $[L_nM]_2(\mu\text{-}P_4)$. They were obtained either from reduction of P_4 by low-valent metal species (uranium[32,33] or zirconium[8]) or upon reduction of alkali phosphides[34] and diphosphane[35] by alkali metals dissolved in liquid ammonia (M = K, Rb, Cs). More recently, Cummins et al. also reported the formation of $\{[(ODipp)_3Nb]_2(\mu\text{-}\eta^3{:}\eta^3P_4)\}$ (Dipp = 2,6-^{i}Pr$_2$C$_6$H$_3$) by P abstraction from a niobium triphosphide precursor.[36] Several tetraphosphane organic derivatives were also described.[37−39]

Recently, we identified new trivalent group 5 imido complexes supported by the bulky 2,6-diisopropylphenyl-β-diketiminate (BDI) ligand.[40,41] These species exhibit an extensive and rich reduction chemistry, including semi-hydrogenation of alkynes[42] and activation of C−F bonds,[43,44] arenes,[45] and azides[46] through unusual pathways. In continuation of this work, we targeted the use of the unsaturated "(BDI)Nb=N^{t}Bu" fragment to achieve early transition metal pnictide complexes. Herein we investigate the reactivity of these Nb and Ta low-valent precursors with white phosphorus. The formation and chemistry of rare diniobium and ditantalum *cyclo*-P_4 inverted sandwich complexes isolable in three different charge states are described. Structural, spectroscopic, and density functional theory (DFT) studies aiming at comparing and determining the precise electronic structure of this series of molecules are also presented.

Received: October 18, 2014
Published: December 3, 2014

   dx.doi.org/10.1021/ja5107282 | J. Am. Chem. Soc. 2014, 136, 17652−17661

RESULTS AND DISCUSSION

Reaction of the trivalent [(BDI)(N^{t}Bu)M(CO)$_2$] (M = Nb, Ta) dicarbonyl precursors[40,41] with white phosphorus afforded the dinuclear inverted sandwich complexes {[(BDI)(N^{t}Bu)-M]$_2$(μ-η^3:η^3P$_4$)} (**1**, M = Nb; **2**, M = Ta) as bright green (**1**) and blue (**2**) crystalline materials in fair yields (Scheme 1). The

Scheme 1. Synthesis of Complexes 1 and 2 from the Dicarbonyl Precursors [(BDI)(N^{t}Bu)M(CO)$_2$] (M = Nb, Ta)

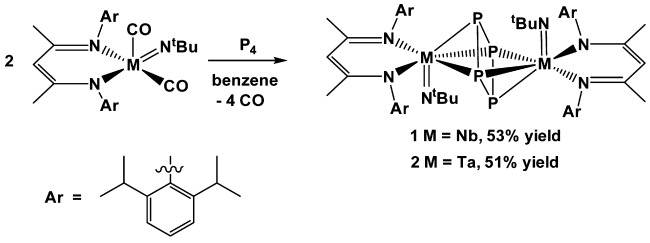

reaction, performed in benzene at 60 °C, proceeded faster in the case of niobium (6 vs 24 h, respectively, for M = Nb vs Ta), which can be attributed to a higher dissociation barrier of the metal−carbonyl bond in the case of Ta. The reaction proceeded faster under UV irradiation, with {[(BDI)(N^{t}Bu)-Ta(CO)$_2$] being converted to **2** in 2 h at room temperature. However, in that case the isolated yield was decreased to 34% due to the formation of several byproducts, as gauged by NMR spectroscopy.

The Nb:P$_4$ ratio had no influence on the reaction, and similar results were obtained when 2:1 to 1:2 Nb:P$_4$ ratios were used. Both species are air-stable and were characterized by ES-MS spectrometry, elemental analysis, UV−vis, and ^{1}H and ^{13}C NMR spectroscopy. The ^{1}H and ^{13}C NMR patterns for **1** and **2** are consistent with highly symmetric diamagnetic species in solution. Despite several attempts performed at various temperatures (−40 to +50 °C), we were unable to locate ^{31}P NMR resonances in the −1000 to +1500 ppm range for either complex in solution. Gratifyingly, the solid-state ^{31}P MAS NMR spectrum recorded at 293 K for **1** displayed two sets of signals (δ_{iso} = +251(2) and +84(2) ppm with large chemical shift anisotropy; see Supporting Information (SI)), corresponding to the two non-equivalent P atoms in the *cyclo*-P$_4$ ligand, in agreement with the asymmetric μ-η^3:η^3 coordination mode observed by X-ray crystallography (see below). In contrast, the previously reported {[(ODipp)$_3$Nb]$_2$(μ-η^3:η^3P$_4$)} complex featured a sharp singlet resonance at +124 ppm in its solution ^{31}P{^{1}H} NMR spectrum.[26] Analysis of the solid-state ^{31}P MAS NMR spectrum for **2** was more difficult because of substantial line-broadening, and we were only able to identify one type of signal at δ_{iso} = +208(8) ppm (see SI).

The solid-state molecular structures of **1** and **2**, determined by single-crystal X-ray diffraction, are shown in Figure 1, and metrical parameters are presented in Table 1. In both cases, the dimeric {[(BDI)(N^{t}Bu)M]$_2$(μ-η^3:η^3P$_4$)} (M = Nb, Ta) unit lies on a crystallographically imposed center of symmetry located in the center of the metal−metal axis. Two independent molecules are found in the asymmetric unit for **1**, and the following discussion uses averaged metrical parameters. The P$_4$ core is nearly a perfect square plane with 0° P−P−P−P torsion angles, P−P−P angles of 88.86(3)° and 88.83(2)° for **1** and **2**, respectively, and almost identical P−P single bonds. The average P−P bond distances found for **1** and **2** (2.233(3) and

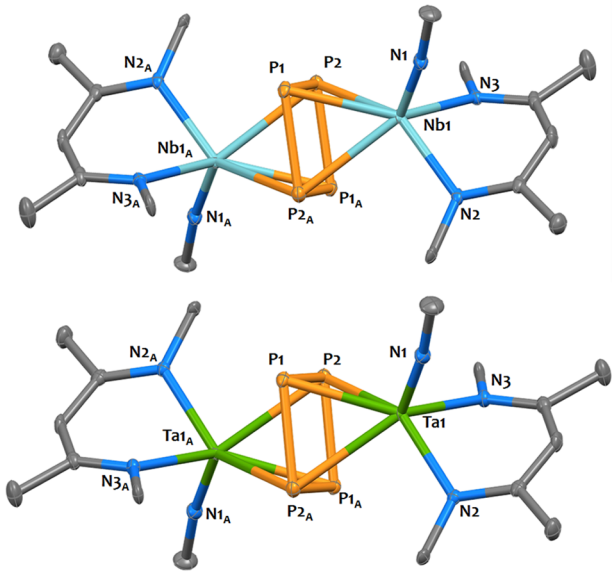

Figure 1. Solid-state molecular structures of **1** (top) and **2** (bottom). Hydrogen atoms and diisopropyl aryl groups of the BDI ligands have been removed, and ^{t}Bu moieties have been truncated for clarity. Niobium (light blue), tantalum (green), phosphorus (orange), nitrogen (blue), and carbon (gray) atoms are represented with 50% probability ellipsoids. Selected metrical parameters are reported in Table 1.

2.248(5) Å, respectively) compare well with those recently reported for (N$_2$P$_2$Zr)$_2$(P$_4$) (2.240(1) Å)[8] and (Dipp-O$_3$Nb)$_2$(P$_4$) (2.23(2) Å),[36] formally described as containing *cyclo*-P$_4^{4-}$ cores. In contrast, shorter P−P distances are found in formally dianionic *cyclo*-P$_4^{2-}$ rings in Cs or U complexes (2.14−2.17 Å, see Results and Discussion below).[32,35] The tetraphosphorus ring is sandwiched between the two metal cations in an unsymmetrical fashion, as expressed by the strong dissymmetry between the M−P distances with, for each metal center, one short (Nb1−P1 = 2.511(1) Å in **1**; Ta1−P1 = 2.5007(1) Å in **2**) and two average (Nb1−P2 = 2.700(1) Å; Nb1−P2A = 2.702(2) Å in **1**; Ta1−P2 = 2.6918(1) Å; Ta1−P2A = 2.6748(1) Å in **2**) metal−phosphorus bond distances. The remaining M−P interaction, located *trans* to the metal imido moiety, is considered as non-bonding with much longer M−P separation (2.845(1) and 2.8179(1) Å for **1** and **2**, respectively), attributed to the *trans* influence of the imido ligand. Therefore, the coordination mode of the *cyclo*-P$_4$ ligand is best described as μ-η^3:η^3. Interestingly, the metal···metal separation is shorter in the case of tantalum (4.2993(1) Å in **2**) compared to niobium (4.3605(1) Å in **1**) and reflects a greater covalent interaction of the tantalum metal centers with the *cyclo*-P$_4$ core. The metrical parameters within the (BDI)M-(N^{t}Bu) unit are unremarkable and similar to those found in related complexes.[40,41,45,47]

The reaction between [(BDI)(N^{t}Bu)M(CO)$_2$] (M = Nb, Ta) and P$_4$ was also attempted in the presence of B(C$_6$F$_5$) in an effort to trap intermediate species, but similar results were obtained.

A more convenient route to **1** involves the hydrogenolysis of the easily accessed bis-dimethyl precursor (BDI)Nb(N^{t}Bu)-Me$_2$[47] in the presence of P$_4$ (Scheme 2). The product precipitated from *n*-hexane solvent to afford **1** in moderate yield after filtration and recrystallization from toluene. Our group has

dx.doi.org/10.1021/ja5107282 | J. Am. Chem. Soc. 2014, 136, 17652−17661

Table 1. Selected Metrical Parameters for Compounds 1, 2, and 4−6 Derived from X-ray Crystallography Data

compd	P−P [Å]	P−P−P [deg]	M−P [Å]	M···M [Å]	Nb=N^{t}Bu [Å]	Nb−N$_{BDI}$ [Å]
1	2.233(3)	88.86(3)	2.51−2.85	4.3605(1)	1.779(2)	2.192(6)
2	2.248(5)	88.83(2)	2.50−2.82	4.2993(1)	1.7912(1)	2.177(7)
4	2.235(2)	88.72(8)	2.52−2.79	4.298(1)	1.775(8)	2.265(6)
5	2.209(4)	89.62(6)	2.59−2.87	4.4929(7)	1.774(4)	2.15(2)
6	2.182(5)	88.9(2)	2.69−2.89	4.61(4)	1.768(6)	2.10(1)

Scheme 2. Formation of 1 and 3 from Hydrogenation of [(BDI)(N^{t}Bu)Nb(Me)$_2$] in the Presence of P$_4$

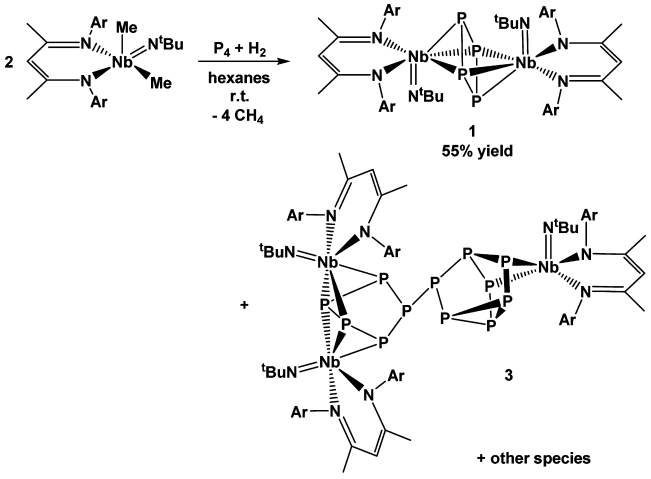

previously shown that the hydrogenation of (BDI)Nb(N^{t}Bu)-Me$_2$ reductively eliminates methane and generates highly reactive low-coordinate Nb(III) intermediates of the general formula "(BDI)Nb(N^{t}Bu)" that can be trapped in the presence of π-acidic ligands such as CO or arenes.[40,45] Therefore, it is likely that the formation of **1** involves the reduction of P$_4$ by these low-valent Nb intermediates generated *in situ*.

The moderate yield of **1** is explained by the formation of several phosphorus-containing byproducts. However, even if the reaction does not exclusively yield {[(BDI)(N^{t}Bu)M]$_2$-(μ-η^3:η^3P$_4$)}, **1** is the main product of the reaction. This selectivity may be partially driven by the relative inertness of compound **1** (see below), which, together with its poorer solubility, facilitates its isolation.

The remaining dark green filtrate contained several by-products, as gauged by NMR spectroscopy. Notably, the ^{1}H NMR spectrum exhibited several signals in the 4.8−5.4 ppm range, corresponding to the *HC*(C(Me)NAr)$_2$ protons of several BDI-Nb species. The ^{31}P NMR spectrum displayed a complicated pattern of resonances between −162 and +184 ppm, attesting that several phosphorus-containing species are formed. Unfortunately, these species exhibited similar solubility and co-crystallized in common solvents (*n*-hexane, benzene, toluene, HMDSO, OEt$_2$); despite several attempts, their separation in preparative scale was unsuccessful, preventing their full analysis.

Even so, fractional recrystallization of the *n*-hexane reaction mixture at −40 °C produced a microcrystalline material whose analysis by ES-MS spectroscopy indicated the presence of a high-nuclearity species, **3**, with a molecular peak at *m*/*z* = 1698.2800 corresponding to [{[(BDI)NbN^{t}Bu]$_3$(P$_{12}$)}-BDI]$^+$. The formation of a trinuclear species was corroborated by the ^{1}H NMR spectrum, which displayed three resonances integrating for one proton each at 5.36, 5.30, and 4.96 ppm and corresponding to three independent BDI ligands within the same molecule.

Analysis by X-ray diffraction revealed a system composed of 12 phosphorus atoms capped by three (BDI)Nb=N^{t}Bu fragments (Figure 2) of the general overall formula {[(BDI)-NbN^{t}Bu]$_3$(μ-P$_{12}$)} (**3**). The architecture of the P$_{12}$ core is unprecedented and can be seen as a P$_7$ cage featuring a nortricyclane-type structure, reminiscent of the well-documented heptaphosphide Zintl anion [P$_7^{3-}$],[48−51] connected to a five-membered *cyclo*-P$_5$ ring. The P−P bond distances vary between 2.146(1) and 2.290(1) Å. These metric values are comparable to those of other known phosphide cages and are in agreement with simple P−P bonds.[51−53] The Nb−P bond lengths range between 2.560(1) and 2.648(1) Å and are shorter in the case of Nb3 (mean Nb−P distance value for Nb3 = 2.564(6) vs 2.62(2) Å for Nb1 and Nb2), which is expected given a lower coordination number for Nb3 compared to those of Nb1 and Nb2.

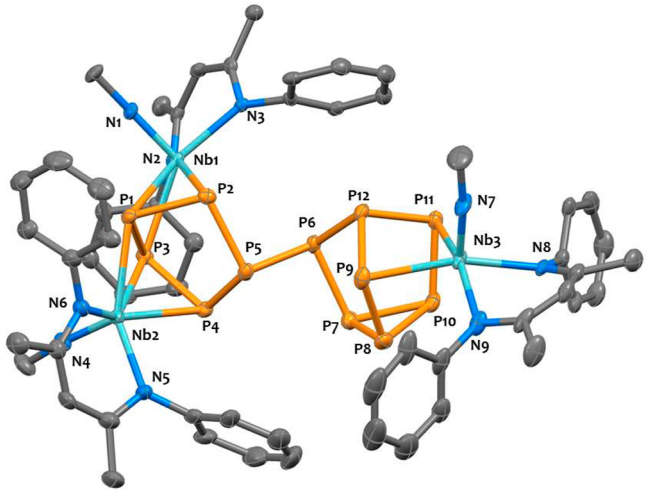

Figure 2. Solid-state molecular structure of **3**. Hydrogen atoms and methyl groups from the ^{t}Bu and ^{i}Pr moieties are omitted for clarity. Niobium (light blue), phosphorus (orange), nitrogen (blue), and carbon (gray) atoms are represented with 50% probability ellipsoids. Selected bond distances [Å] and angles [°]: Nb1−P1 2.622(1), Nb1−P2 2.623(1), Nb1−P3 2.648(1), Nb2−P1 2.623(1), Nb1−P3 2.575(1), Nb1−P4 2.622(1), Nb3−P11 2.569(1), Nb3−P9 2.560(1), Nb1−N1 1.747(3), Nb1−N2 2.206(3), Nb1−N3 2.182(3), Nb2−N4 1.763(3), Nb2−N5 2.188(3), Nb2−N6 2.198(3), Nb3−N7 1.754(3), Nb3−N8 2.234(3), Nb3−N9 2.220(3), P−P bond length range 2.146(1)−2.290(1).

Phosphorus has a proclivity for homoatomic bonding,[51−54] and activation of P$_4$ by transition metal species can lead to various P$_n$ (n > 4) species upon aggregation of smaller fragments. However, clusters of nuclearity above n = 7 are obtained only on very rare occasions.[4,18] To date, only two other P$_{12}$ clusters possessing different topologies have been

dx.doi.org/10.1021/ja5107282 | J. Am. Chem. Soc. 2014, 136, 17652−17661

described. Bertrand reported the high-yield synthesis of a HNC-capped P_{12} cluster from P_4,[55] and the structure of the trinuclear cobalt $\{(Cp')Co]_3(\mu\text{-}P_{12})\}$ (Cp' = 1,2,4-^{t}BuC$_5$H$_2$) complex was elucidated from ^{31}P NMR spectroscopy by Scherer et al.[56] In the present case, **1** was found unreactive toward P_4, and **3** is therefore not the result of P_4 incorporation into **1**. Unfortunately, separation of **3** from the other reaction byproducts failed in our hands, preventing further analysis of this compound.

In an attempt to find a more efficient method for the preparation of compound **2**, we investigated the hydrogenolysis of the tantalum dimethyl complex (BDI)Ta(N^{t}Bu)Me$_2$ in the presence of P_4. However, the outcome was quite different from that observed for its Nb counterpart. Indeed, the major product of the reaction was the cyclometalated tantalum hydride species {ArNC(Me)CHC(Me)N-[2-(CHMeCH$_2$)-6-^{i}Pr-C$_6$H$_3$]}Ta-(N^{t}Bu)H, as assayed by NMR spectroscopy, similar to what we previously reported for the same reaction performed in the absence of white phosphorus.[41]

Reactivity Studies. Compound **1** is fairly robust and can be handled in air either in the solid state or in solution. The *cyclo*-P_4 ring was not hydrogenated in the presence of H_2 and was not displaced by strong π-acidic ligands such as CO.

In order to determine if the coordinated *cyclo*-P_4 exhibited basic properties, we explored the reaction of **1** with 2 equiv of [HOEt$_2$][B(C$_6$F$_5$)$_4$]. The reaction produced a new compound formulated as $\{[(BDI^{\#})Nb(N^tBu)]_2(\mu\text{-}\eta^3\text{:}\eta^3P_4)\}[B(C_6F_5)_4]_2$ (**4**), in which the BDI backbone has been protonated (Scheme 3, BDI$^{\#}$ = [ArNC-(Me)]$_2$CH$_2$). Compound **4** can be isolated in

Scheme 3. Formation of 4 (Ar = 2,6-Diisopropylphenyl; Ar^F = Pentafluorophenyl)

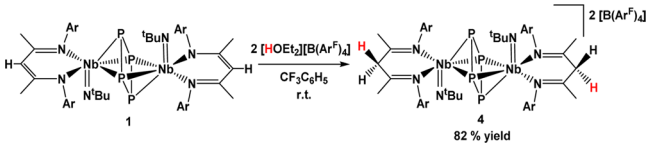

high yields as pink crystals. Because of its ion-pair formulation, **4** has poor solubility in hydrocarbon solvents, Et$_2$O, CH$_2$Cl$_2$, and CHCl$_3$, but is fairly soluble and stable in (CH$_2$Cl)$_2$. In addition, **4** was found to decompose in polar coordinating solvents such as THF or pyridine to yield a complex mixture of unidentified products. Protonation of the BDI ligand was confirmed by the ^{1}H NMR spectrum for **4**, which displays two doublets at 5.44 and 4.68 ppm ($^2J_{HH}$ = 16.7 Hz) that couple in the ^{1}H−^{1}H COSY NMR spectrum, corresponding to the two diastereotopic CH$_2$ protons in H$_2$C(C(Me)NAr)$_2$.

Further confirmation of the molecular structure of **4** was obtained by single-crystal X-ray crystallography. The structure consists of ion pairs with two BAr^F counteranions balancing the charge of the $\{[(BDI^{\#})(N^tBu)Nb]_2(\mu\text{-}\eta^3\text{:}\eta^3P_4)\}^{2+}$ dicationic complex shown in Figure 3. Selected metrical parameters are given in Table 1. The CH$_2$ protons in H_2C(C(Me)NAr)$_2$ were located from the Fourier difference map and refined isotropically. The H_2C(C(Me)NAr)$_2$ ligand core is no longer planar, with the sp^3-hybridized methylene carbon lying at 0.51(1) Å below the plane defined by the two C═N imino moieties. The C═N bond lengths are short (1.286(6) Å), in agreement with localized double imine bonds. As a consequence of the β-diketiminate protonation, the interaction between the niobium center and the neutral BDI$^{\#}$ ligand is weakened compared to

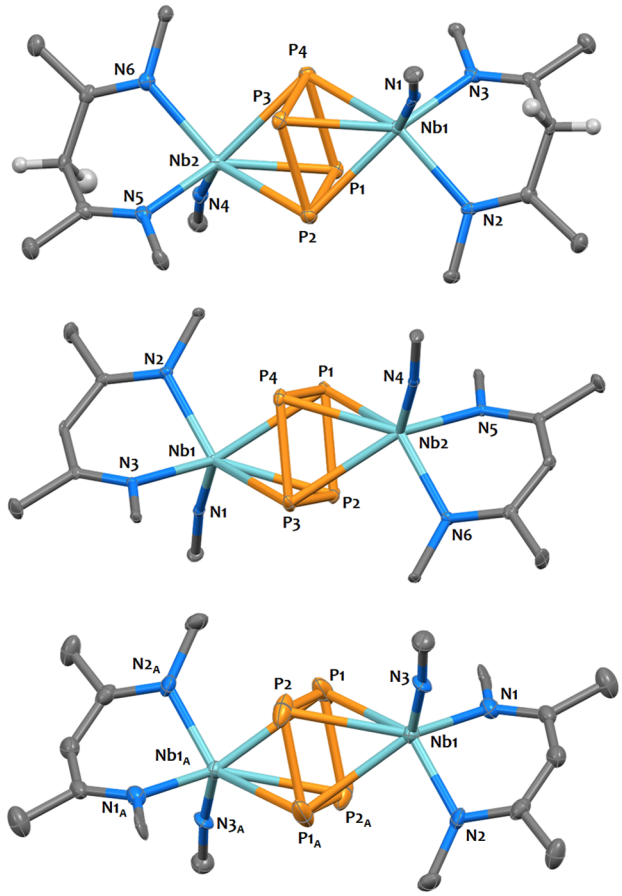

Figure 3. Solid-state molecular structures of **4** (top), **5** (middle), and **6** (bottom). Hydrogen atoms are not shown except for those of the methylene group of the protonated BDI$^{\#}$ ligand in **4**, diisopropyl aryl groups of the BDI ligands and B(C$_6$F$_5$)$_4$ counteranions have been removed, and ^{t}Bu moieties have been truncated for clarity. Niobium (light blue), phosphorus (orange), nitrogen (blue), hydrogen (white), and carbon (gray) atoms are represented with 50% probability ellipsoids. Selected metrical parameters are reported in Table 1.

that found in **1**, with longer Nb−N bond distances in **4** (2.265(6) Å) than in **1** (2.192(6) Å). This results in a stronger Nb-*cyclo*-P_4 interaction in **4**, as shown by the shorter Nb···Nb separation (4.298(1) Å in **5** vs 4.3605(1) Å in **1**), while the geometry of the tetraphosphorus core is essentially unchanged, with similar phosphorus−phosphorus bond distances and angles in **1** and **4** (see Table 1). The average Nb═N^{t}Bu imido bond length in **5** (1.775(8) Å) is similar to that found for **1**.

To probe possible nucleophilicity, **1** was treated with acyl chlorides but did not react and was not affected by the strong Lewis acid B(C$_6$F$_5$)$_3$. Overall, the lack of reactivity of the *cyclo*-P_4 unit with Brønsted and Lewis acids might reflect the poor basicity/nucleophilicity of the tetraphosphide in **1**, but this may as well be a kinetic effect due to the steric protection provided by the bulky BDI ligands; note that we previously reported analogous behavior with the arene inverted sandwich complex $\{[(BDI)Nb(N^tBu)]_2(\mu\text{-}\eta^6\text{:}\eta^6C_6H_6)\}$.[45]

Although the niobium centers in **1** can *formally* be described as d^0 metal centers, the overall molecule should be considered electron-rich and can therefore be easily oxidized.

The reaction between **1** and 1 equiv of Ag[B(C$_6$F$_5$)$_4$] proceeded quickly at room temperature in toluene and afforded

dx.doi.org/10.1021/ja5107282 | J. Am. Chem. Soc. 2014, 136, 17652−17661

an insoluble dark green material. Complex $\{[(BDI)(N^tBu)Nb]_2(\mu\text{-}\eta^3\text{:}\eta^3P_4)\}\{B(C_6F_5)_4\}$ (**5**) was isolated in 77% yield upon extraction of the solid residue with α,α,α-trifluorotoluene and crystallization by *n*-hexane layering. In return, **5** could be quantitatively reduced back to **1** using 1 equiv of bis(cyclopentadienyl)cobalt(II) (as assayed by ^{1}H NMR spectroscopy, Scheme 4). The ^{1}H NMR spectrum for **5** displays several

Scheme 4. Redox Chemistry of 1

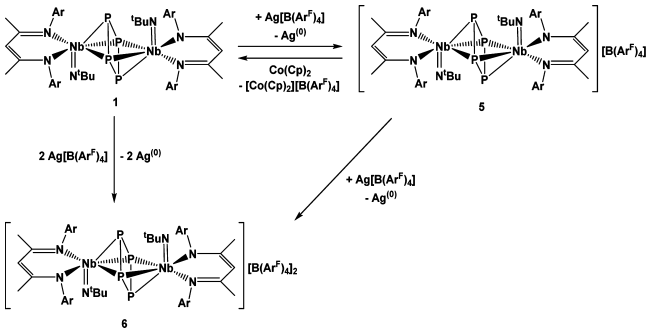

broad, unassignable features from −0.8 to +8.9 ppm that remain broad over the −50 to +60 °C temperature range, and no ^{31}P NMR signals could be located. This is attributed to the paramagnetic nature of this $S = {}^1/_2$ radical species (see EPR study below).

The two-electron oxidation product, $\{[(BDI)(N^tBu)Nb]_2(\mu\text{-}\eta^3\text{:}\eta^3P_4)\}\{B(C_6F_5)_4\}_2$ (**6**), was isolated in 64% yield from an analogous reaction performed with greater than 2 equiv of the silver oxidizing agent. This ion-pair compound is insoluble in most conventional solvents. **6** is either poorly soluble or reactive with most solvents, but it is sufficiently stable in α,α,α-trifluorotoluene to obtain ^{1}H and ^{31}P NMR spectra. The ^{1}H NMR spectrum for **6** features the expected BDI resonances for a symmetric diamagnetic species in solution. Contrary to **1**, **6** displays a sharp singlet resonance in its ^{31}P NMR spectrum at +516 ppm, which indicates that all the phosphorus atoms of the *cyclo*-P_4^{2-} moiety are equivalent on the NMR time scale. This resonance is shifted significantly downfield compared to that of the previously reported M_2P_4 species (δ = +331−348 ppm for M = K, Rb, Cs).

Interestingly, the choice of the counteranion of the Ag(I) salt turned out to be crucial: use of $Ag[BF_4]$ in place of $Ag[B(C_6F_5)_4]$ resulted in a complex mixture of products, as gauged by ^{1}H NMR spectroscopy. Analysis of the reaction mixture by ^{19}F NMR showed a broad resonance centered at +83 ppm which corresponds to the previously reported Nb(V) difluoride species $[(BDI)(N^tBu)NbF_2]$.[47] This likely arises from fluoride abstraction from tetrafluoroborate by a cationic Nb species. Alternatively, when triflate was used in place of the non-coordinating tris-pentafluoroborate anion, the pentavalent niobium triflate species $[(BDI)(N^tBu)Nb(OTf)_2]$ (**7**) was isolated as yellow crystals in 24% yield. Compound **7** was fully characterized by multinuclear NMR spectroscopy, elemental analysis, IR, and X-ray diffraction (see SI). The formation of **7** most likely involves a reactive intermediate which undergoes ligand exchange in the presence of coordinating triflate anions. However, attempts to isolate or characterize by ^{31}P NMR the byproduct(s) were unsuccessful.

Here we consider it appropriate to draw a parallel between the present *cyclo*-P_4 inverted sandwich species and the related benzene inverted sandwich species $\{[(BDI)Nb(N^tBu)]_2(\mu\text{-}\eta^6\text{:}\eta^6\text{-}C_6H_6)\}$, which is best described as a diniobium(III) complex with strong Nb−arene back-donation.[45] In the latter case, and contrary to what is observed for **2**, we observed that the two-electron oxidation is irreversible and the arene-bridged complex decomposes.[57] This difference in reactivity can be ascribed to a stronger interaction and stronger orbital overlap with the *cyclo*-P_4 ring vs C_6H_6. This is also consistent with the fact that benzene does not displace CO in the dicarbonyls $[(BDI)(N^tBu)M(CO)_2]$ (M = Nb, Ta), while P_4 does.

Structural Comparisons. The isolation of a family of closely related systems in several charge states provides a rare opportunity for comparing their structures and physicochemical properties. Both **5** and **6** were structurally characterized by single-crystal X-ray diffraction (Figure 3). As in the structure of **1**, each niobium atom in **5** and **6** is coordinated by a bidentate (BDI) ligand, a (N^tBu) imido fragment bound in a terminal fashion, and a planar η^3:η^3-bridging *cyclo*-P_4 ring perpendicular to the Nb−Nb axis. The three structures differ in their charge state, resulting in the presence of one and two BAr^F counterions in the structures of complexes **5** and **6**, respectively.

In Table 1, the most relevant structural parameters for the *cyclo*-P_4 species **1**, **2**, and **4**−**6** are reported. The geometry of the P_4 motif is an almost perfect square plane across the series, with P−P−P angles close to 90 °C (see Table 1). The P−P bond lengths within each P_4 core show very little deviation, and therefore the discussion is based on an averaged value for each species. Comparison of the P−P distances shows very significant differences: specifically, the average P−P bond length is almost identical (within esd's) in **1** and **4** (2.234 Å), both containing a formally *cyclo*-P_4^{4-} core, but is shortened by around 0.03 Å in **5** (2.209(4) Å) and by another 0.03 Å in **6** (2.182(5) Å). Such distances compare well to those found in other systems containing the reduced *cyclo*-P_4 motif and seem diagnostic of its formal charge state, with values ranging from 2.22 to 2.25 Å for tetraanionic rings[8,36] and from 2.14 to 2.20 Å for dianionic rings.[32,33,35] The degree of interaction between the metal center and the bridging tetraphosphide is also very dependent on the oxidation state. Overall, shorter Nb−P bond distances are found in the reduced species **1** compared to **6**, although these span an extended range because of the asymmetric coordination mode of the P_4 core. This is best seen when comparing the Nb···Nb separation, which increases significantly from 4.3605(1) Å in **1** to 4.4929(7) Å in **5** and 4.61(4) Å in **6**. This is compensated by a stronger donation from the BDI backbone and, to a lesser extent, from the imido ligand to the d^0 metal centers, as expressed by a shortening of the Nb−N_{BDI} distances (2.192(6) Å in **1** vs 2.10(1) Å in **6**). Hence, as expected, the data show that increasing the charge on the central *cyclo*-P_4 ring results in a more contracted $[Nb_2P_4]$ core.

Computational Analysis. Although it is convenient to refer to formal charges when describing these systems, the nature of metal−phosphorus bonding is essentially covalent. We thus turned to DFT calculations to get a better comprehension of their electronic structure.

Geometry optimizations were carried out without any symmetry constraints on complexes **1**, **2**, **4**−**6** using the B3PW91 functional (see SI for computational details). This functional is found to correctly account for the structural features of the five investigated complexes (see SI for metric comparison with X-ray data). The maximum deviation of the P−P bonds is around 0.04 Å, whereas the P−P−P angles are

dx.doi.org/10.1021/ja5107282 | J. Am. Chem. Soc. 2014, 136, 17652−17661

perfectly reproduced. The unsymmetrical coordination of P_4 to the two metal centers is also reproduced computationally. Thus, these computational methods appear to be well suited to further study the electronic and spectroscopic properties of these complexes (see below). Since an unsymmetrical coordination of P_4 to the two Nb centers is found in **1**, any attempt to analyze atomic charges is questionable. Thus, a NBO analysis was carried out. Analysis of the Wiberg bond indexes (WBO) points in the direction of formally Nb(V) metal centers and a P_4^{4-} ligand. Indeed, for one Nb center, two interactions with the BDI ligand (WBO = 0.51), one interaction with the imido (WBO = 1.93), and four interactions with the four phosphorus (WBO = 0.88, 0.64, 0.64, and 0.37) are found, as well as a weak Nb−Nb interaction (WBO = 0.23).

The analysis of the molecular orbitals in **1**, **2**, and **4** shows that the HOMO is a δ-bonding orbital involved in the covalent bonding between the metal centers and the P_4 ring, while the electron density in the non-bonding LUMO is essentially localized on metal d-orbitals. (See Figure 4 for a representation of the HOMO and LUMO orbitals in **1**.)

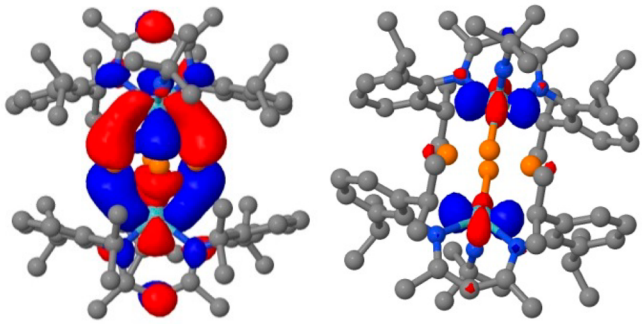

Figure 4. HOMO (left) and LUMO (right) orbitals of complex **1**.

In **5**, the coordination is slightly less strong, in line with longer Nb−P bond distances. Indeed, for one Nb center, the two interactions with the BDI ligand (WBO = 0.57) and the one with the imido (WBO = 1.95) are equivalent (even slightly stronger) to those in complex **1**, but the four interactions with the four phosphorus (WBO = 0.71, 0.52, 0.52, and 0.36) as well as the Nb−Nb one (WBO = 0.12) are weakened.

EPR Spectroscopy. The room-temperature X-band EPR spectrum of **5** was nicely resolved and could be satisfactorily simulated: both experimental and simulated spectra are presented in Figure 5. The spectrum is isotropic and is defined by a single g value, g_{iso} = 2.041. The 19 equally spaced lines and splitting pattern suggest that the spin is delocalized onto two equivalent Nb centers. Accordingly, the spectrum was modeled with a hyperfine interaction of 41.5 G, with two equivalent ^{93}Nb nuclei (100% natural abundance, $I = {}^9/_2$). No evidence for superhyperfine couplings with the $I = {}^1/_2$ ^{31}P nuclei could be detected.

Using DFT methods, it has been possible to derive the spin density of complex **5**, which was computed as a doublet spin state, yielding an extra α spin. The spin density is found to be mainly located on the two Nb centers (more than 0.6 electron), with the remaining 0.4 electron delocalized over the different ligands. The spin density is symmetrically distributed over the two Nb centers, in agreement with the EPR experiment. This observation is in stark contrast to that of $\{[(BDI)(N^tBu)Nb]_2(\mu\text{-}C_6H_6)\}\{BAr^F\}$, where the single electron is not delocalized

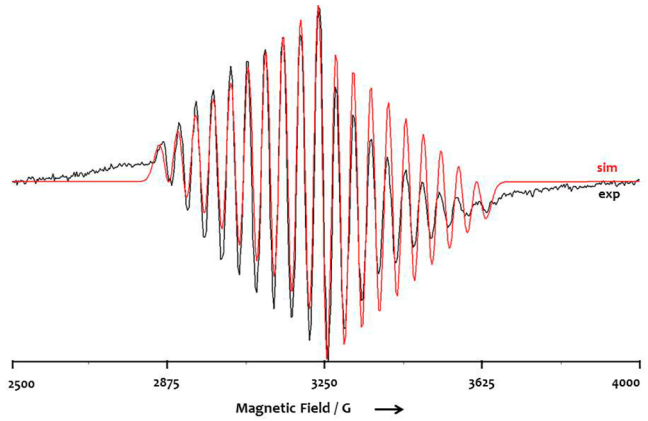

Figure 5. Room-temperature liquid-solution ($CF_3C_6H_5$) X-band EPR spectrum of **5** (black line) and simulation (red line). Hyperfine coupling constant: A_{iso} = 41.5 G (^{93}Nb, 100% natural abundance, $I = {}^9/_2$); g_{iso} = 2.041.

equally onto both niobiums, resulting in a more complex EPR signal.[57] The more isotropic and equal distribution of the spin density in **5** suggests better orbital overlap.

Optical Spectra. The optical spectra of the formally *cyclo*-P_4^{4-} species **1**, **2** (recorded in toluene solution), and **4** (recorded in dichloroethane) feature two types of intense absorptions (Figure 6). High-intensity (20 000 < ε < 37 000 L·

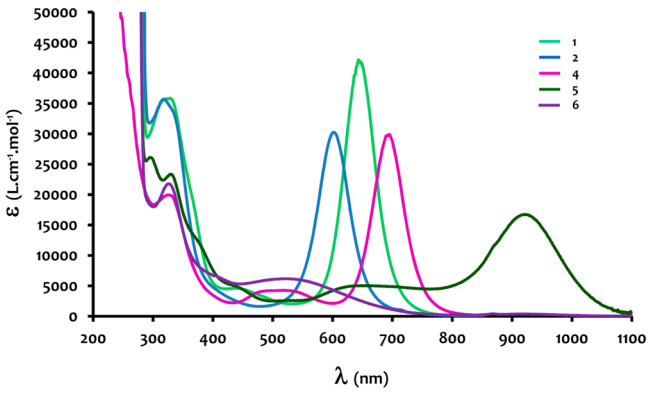

Figure 6. Solution UV−visible absorption spectra (298 K) of complexes **1** (bright green line, toluene), **2** (blue line, toluene), **4** (fuchsia line, DCE), **5** (dark green line, $CF_3C_6H_5$), and **6** (purple line, $CF_3C_6H_5$).

$cm^{-1}\cdot mol^{-1}$) bands are observed in the UV region around 320 nm that we attribute to intraligand $\pi\rightarrow\pi^*$ transitions. Additionally, **1**, **2**, and **4** display strong absorption bands (29 000 < ε < 42 000 $L\cdot cm^{-1}\cdot mol^{-1}$) in the visible region (λ = 645, 603, and 694 nm for **1**, **2**, and **4**, respectively) responsible for the bright colors of these molecules. Given their high intensities, it is unlikely that these correspond to Laporte-forbidden d→d transitions. Instead, we attribute these processes to phosphorus-to-metal charge-transfer transitions. The energy for this transition is strongly affected both by the nature of the metal center (Ta vs Nb) and by the supporting ligand (BDI vs BDI$^{\#}$) and is therefore a useful tool to probe the nature of the metal−*cyclo*-P_4 interaction.

Time-dependent density functional theory (TD-DFT) calculations were carried out to further probe the nature of these transitions. The calculated λ_{max} values (see table in SI) are in good agreement with the experimental values and

dx.doi.org/10.1021/ja5107282 | J. Am. Chem. Soc. 2014, 136, 17652−17661

correspond to a HOMO−LUMO excitation. Upon analysis of the nature of the HOMO and LUMO orbitals involved in the excitation, it appears that the transition can be described as a pseudo-charge transfer between the *cyclo*-P_4 ligand (HOMO) and the metal centers (LUMO). While **1** and **2** exhibit similar electron configurations, this transition for **2** is radically blue-shifted in comparison with that for **1**. DFT shows an increased stabilization of the HOMO δ-bonding orbital in the case of tantalum due to increased covalency, resulting in a larger HOMO−LUMO gap in **2**, as observed by UV−visible spectroscopy. This is also in agreement with the X-ray structural data, which show shorter Ta−P bonds in **2** than Nb−P bonds in **1** (see above).

The optical spectrum for the radical cation species **5** features ligand $\pi\rightarrow\pi^*$ transitions in the UV region as well as a broad and intense (ε = 22 750 L·cm^{-1}·mol^{-1}) absorption band at low energy (λ = 921 nm, Figure 6). The nature of the frontier orbitals involved in this transition indicates that there is an electronic rearrangement between the SOMO (mainly based on a bonding Nb−P−P−Nb interaction) and the LUMO (non-bonding interaction between the two Nb centers). As a consequence of the depopulation of the Nb−P_4−Nb δ-bonding orbital, no such intense transition is observed in the symmetric fully oxidized dication complex **6**. Instead, the absorption spectrum for **6** shows a broad feature centered at λ = 522 nm (ε = 6160 L·cm^{-1}·mol^{-1}), corresponding to a transition from BDI-Nb bonding orbitals (HOMO−10, HOMO−8) to the LUMO (non-bonding interaction between one d-orbital located on each Nb).

CONCLUSIONS

We have shown that low-coordinate d^2 Nb and Ta complexes supported by a combination of imido and β-diketiminate ligands result in a strong activation of P_4 to yield unusual *cyclo*-tetraphosphide-bridged inverted sandwich complexes. The structure of an unprecedented P_{12} cluster byproduct was also determined. Interestingly, the reaction of $[(BDI)Nb(N^tBu)]_2$-(μ-η^3:η^3P_4) with $[HOEt_2][B(C_6F_5)_4]$ was found to result in the protonation of the BDI ligand rather than the phosphide ring.

We have demonstrated for the first time that the *cyclo*-P_4 motif can exist in various oxidation states within the same system. Specifically, salts of the $\{[(BDI)(N^tBu)Nb]_2$-(μ-η^3:η^3P_4)$\}^{n+}$ (n = 1, 2) mono- and dication were isolated. This offered us the rare opportunity to compare the physicochemical properties of a family of structurally related compounds. The combined chemical, structural, spectroscopic, and density functional theory analyses suggest that the best description for these complexes is as high-valent Nb centers with substantial covalent bonding with the *cyclo*-P_4 core. They also revealed that the metal−phosphorus interaction was stronger for Ta than for Nb, and that it was weakened upon oxidation. An increased reactivity is thus expected for the cationic species reported in this work; studies aimed at determining the full scope of reactivity of these species are currently being pursued. In addition, future work will be directed toward the expansion of these studies to encompass niobium imido systems supported by sterically modified BDI as well as other bidentate ligands in order to elucidate the role played by steric and electronic factors in the formation and the kinetic stability of these species.

EXPERIMENTAL SECTION

General Considerations. Unless otherwise noted, all reactions were performed either using standard Schlenk line techniques or in an MBraun inert atmosphere glovebox under an atmosphere of purified nitrogen (<1 ppm of O_2/H_2O). Glassware and cannulae were stored in an oven at ~160 °C for at least 12 h prior to use. Toluene, *n*-hexane, THF, and benzene were purified by passage through a column of activated alumina, stored over 3 or 4 Å molecular sieves, and degassed prior to use. α,α,α-Trifluorotoluene and dichloroethane were dried over P_2O_5, distilled under reduced pressure, degassed, and stored over 4 Å molecular sieves. C_6D_6 was dried over sodium/benzophenone, and $CDCl_3$ was dried over CaH_2. The deuterated solvents were then vacuum-transferred to a storage flask and degassed before being stored over activated molecular sieves in a drybox. $(BDI)(CO)_2Nb(N^tBu)$,[40] $(BDI)(CO)_2Ta(N^tBu)$,[41] and $(BDI)(Me)_2Nb(N^tBu)$[47] were prepared using literature procedures. White phosphorus (P_4) was prepared from red phosphorus thermolysis under vacuum.[58] All other reagents were acquired from commercial sources and used as received. NMR spectra were recorded on Bruker AV-300, AVQ-400, AVB-400, DRX-500, AV-500, and AV-600 spectrometers. Chemical shifts were measured relative to residual solvent peaks, which were assigned relative to an external TMS standard set at 0.00 ppm. ^{31}P and ^{19}F chemical shifts were referenced to an external standard (Ph_3PO for ^{31}P set at 23 ppm and $BF_3{\cdot}OEt_2$ for ^{19}F set at 0.00 ppm). ^1H and ^{13}C NMR assignments were routinely confirmed by ^1H−^1H COSY and ^1H−^{13}C HSQC experiments. Samples for UV−vis−NIR spectroscopy were prepared in a Schlenk-adapted quartz cuvette and analyzed on a Varian Cary 50 scanning spectrophotometer. The uncorrected melting points were determined using sealed capillaries prepared under nitrogen on an Optmelt SRS. Elemental analyses were performed either at the School of Human Sciences, Science Center, London Metropolitan University, or at the College of Chemistry, University of California, Berkeley. The X-ray structural determinations were performed at CHEXRAY, University of California, Berkeley, on a Bruker SMART APEX II QUAZAR diffractometer. Solution EPR spectra were collected at 9.251 GHz (X-band) frequency at room temperature in $CF_3C_6H_5$ using a Varian E-109 spectrometer equipped with an E-102 microwave bridge. The EPR spectra were simulated and optimized using WinSim.[59] Mass spectra were acquired on a Finnigan LTQ FT mass spectrometer equipped with an ESI source. THF and *n*-hexane solutions were prepared and filtered in the glovebox and maintained under a nitrogen atmosphere until injection in the spectrometer through a syringe pump. Mass spectra were recorded over a mass range (m/z) of 400−2000 with a Fourier transform ion cyclotron resonance (FT-ICR) MS detector, while MS/MS data were obtained with a linear ion trap (LTQ) analyzer. The exact mass and experimental isotopic profiles were compared in each case to the theoretical ones. Details concerning X-ray diffraction analyses and DFT computational studies are provided in the SI.

Synthetic Methods. *{[(BDI)Nb(N^{t}Bu)]$_2$(μ-η^3:η^3P$_4$)} (**1**). Method A: From [(BDI)(CO)$_2$Nb(N^{t}Bu)].* A 0.5 mL benzene solution of $[(BDI)(CO)_2Nb(N^tBu)]$ (29.9 mg, 0.047 mmol, 1 equiv) and P_4 (5.8 mg, 0.047 mmol, 1 equiv) was heated to 60 °C for 6 h. The resulting dark green suspension was allowed to cool to room temperature, giving dark green crystals of **1** that were recovered by filtration and dried *in vacuo* (16.0 mg, 0.012 mmol, 53% yield). Dark green-red dichroic block-shaped single crystals suitable for X-ray diffraction were obtained upon recrystallization from toluene. ^1H NMR (400 MHz, $CDCl_3$, 293 K): δ = 6.85 (t, 2H, *p*-Ar, $^3J_{HH}$ = 7.6 Hz), 6.73 (dd, 4H, *o,m*-Ar, $^3J_{HH}$ = 7.7 Hz), 5.46 (s, 1H, *H*C(C(Me)NAr)$_2$), 3.72−3.63 (sept, 2H, C*H*Me$_2$, $^3J_{HH}$ = 6.7 Hz), 3.51−3.42 (sept, 2H, C*H*Me$_2$, $^3J_{HH}$ = 6.7 Hz), 1.82 (s, 6H, HC(C(*Me*)NAr)$_2$), 1.49 (s, 9H, N^t*Bu*), 1.06 (d, 6H, CH*Me*$_2$, $^3J_{HH}$ = 6.7 Hz), 1.03 (d, 6H, CH*Me*$_2$, $^3J_{HH}$ = 6.8 Hz), 0.96 (d, 6H, CH*Me*$_2$, $^3J_{HH}$ = 6.7 Hz), 0.33 (d, 6H, CH*Me*$_2$, $^3J_{HH}$ = 6.6 Hz). ^1H NMR (400 MHz, C_6D_6, 293 K): δ = 6.98 (m, 2H, *p*-Ar), 6.90−6.87 (m, 4H, *o,m*-Ar), 5.29 (s, 1H, *H*C(C(Me)NAr)$_2$), 3.95−3.85 (sept, 2H, C*H*Me$_2$, $^3J_{HH}$ = 6.7 Hz), 3.72−3.62 (sept, 2H, C*H*Me$_2$, $^3J_{HH}$ = 6.7 Hz), 1.72 (s, 9H, N^t*Bu*), 1.69 (s, 6H, HC(C(*Me*)NAr)$_2$), 1.25 (d, 6H, CH*Me*$_2$, $^3J_{HH}$ = 6.7 Hz), 1.23 (d, 6H, CH*Me*$_2$, $^3J_{HH}$ = 6.7 Hz), 1.16 (d,

dx.doi.org/10.1021/ja5107282 | J. Am. Chem. Soc. 2014, 136, 17652−17661

6H, CH*Me*$_2$, $^3J_{HH}$ = 6.7 Hz), 0.61 (d, 6H, CH*Me*$_2$, $^3J_{HH}$ = 6.7 Hz). $^{13}C\{^1H\}$ NMR (125.8 MHz, $CDCl_3$, 293 K): δ = 170.25 (C, HC(*C*(Me)NAr)$_2$), 152.25 (C, Ar), 142.05 (C, Ar), 141.08 (C, Ar), 125.46 (CH, Ar), 124.89 (CH, Ar), 123.35 (CH, Ar), 104.61 (CH, HC(C(Me)NAr)$_2$), 33.00 (CH$_3$, Nb═N^t*Bu*), 28.43 (CH, ^{i}Pr), 27.25 (CH, ^{i}Pr), 25.78 (CH$_3$, ^{i}Pr), 25.72 (CH$_3$, ^{i}Pr), 25.35 (CH$_3$, ^{i}Pr), 25.21 (CH$_3$, ^{i}Pr), 23.84 (CH$_3$, HC(C(*Me*)NAr)$_2$). ^{31}P MAS NMR (202 MHz, 293 K): δ_{iso} = 251, 84. FT-IR (cm^{-1}): 2966 (w), 2864(w), 1515 (s), 1434 (m), 1382 (s), 1362 (s), 1312 (s), 1257 (m), 1226 (s), 1169 (m), 1108 (m), 1013 (s), 933 (s), 847 (s), 793 (s), 773 (m), 756 (m). UV−vis (toluene): λ_1 = 325 nm (ε = 36 000 L·cm^{-1}·mol^{-1}); λ_2 = 440 nm (ε = 4900 L·cm^{-1}·mol^{-1}); λ_3 = 645 nm (ε = 42 000 L·cm^{-1}·mol^{-1}). ES-MS: *m*/*z* = 1286.5095 [M]$^+$ (calcd for $C_{66}H_{100}N_6P_4Nb_2$: 1286.5093). Anal. Calcd for $C_{66}H_{100}N_6Nb_2P_4$: C, 61.58; H, 7.83; N, 6.53. Found: C, 61.47; H, 7.86; N, 6.71. mp >400 °C.

Method B: From [(BDI)(CH$_3$)$_2$Nb(N^{t}Bu)]. H_2 (1 atm) was added to a 250 mL *n*-hexane solution of [(BDI)(CH$_3$)$_2$Nb(N^{t}Bu)] (2.28 g, 3.73 mmol, 1 equiv) and P_4 (0.28 g, 2.23 mmol, 0.6 equiv). The reaction mixture immediately turned green and then was stirred at room temperature for 12 h to give a dark green suspension. The *n*-hexane fraction was filtered, and the solid residue was recrystallized from toluene, giving **1** as a dark green crystalline solid (1.33 g, 1.03 mmol, 55%). The dark green *n*-hexane solution was left to stand at −40 °C overnight, producing a green microcrystalline material. Analysis by ^1H NMR (500 MHz, C_6D_6, 293 K) showed the formation of several byproducts and notably three resonances at δ = 5.36 (s, 1H, *H*C(C(Me)NAr)$_2$), 5.30 (s, 1H, *H*C(C(Me)NAr)$_2$), and 4.96 (s, 1H, *H*C(C(Me)NAr)$_2$), attributed to **4**. Fractional recrystallization from *n*-hexane at −40 °C afforded dark green crystals of **4** suitable for X-ray diffraction. ES-MS: *m*/*z* = 1698.2800 [{[(BDI)NbN^{t}Bu]$_3$(P$_{12}$)}-BDI]$^+$ (calcd for $C_{70}H_{109}N_7Nb_3P_{12}$: 1698.2787). Successive recrystallizations failed to separate **4** from co-crystallized byproducts, preventing full analysis.

{[(BDI)Ta(N^{t}Bu)]$_2$(μ-η^3:η^{3}P$_4$)} ***(2)***. A 100 mL benzene solution of [(BDI)(CO)$_2$Ta(N^{t}Bu)] (200 mg, 0.276 mmol, 2 equiv) and P_4 (34 mg, 0.276 mmol, 1 equiv) was heated to 60 °C for 24 h. The resulting dark blue/green suspension was allowed to cool to room temperature, giving dark blue crystals of **2** that were recovered by filtration, washed with 0.5 mL of *n*-hexane, and dried *in vacuo* (103 mg, 0.070 mmol, 51% yield). Dark blue block-shaped single crystals suitable for X-ray diffraction were obtained upon recrystallization from benzene. ^1H NMR (500 MHz, C_6D_6, 293 K): δ = 6.96 (t, 2H, *p*-Ar, $^3J_{HH}$ = 7.6 Hz,), 6.89 (dd, 4H, *o*,*m*-Ar, $^3J_{HH}$ = 7.6, 2.3 Hz), 5.37 (s, 1H, *H*C(C(Me)NAr)$_2$), 4.13−4.05 (sept, 2H, C*H*Me$_2$, $^3J_{HH}$ = 6.7 Hz), 3.63−3.55 (sept, 2H, C*H*Me$_2$, $^3J_{HH}$ = 6.7 Hz), 1.69 (s, 9H, N^t*Bu*), 1.67 (s, 6H, HC(C(*Me*)NAr)$_2$), 1.27 (d, 6H, CH*Me*$_2$, $^3J_{HH}$ = 6.7 Hz), 1.17 (d, 6H, CH*Me*$_2$, $^3J_{HH}$ = 6.8 Hz), 1.13 (d, 6H, CH*Me*$_2$, $^3J_{HH}$ = 6.7 Hz), 0.61 (d, 6H, CH*Me*$_2$, $^3J_{HH}$ = 6.6 Hz). ^1H NMR (600 MHz, $CDCl_3$, 293 K): δ = 6.85 (t, 2H, *p*-Ar, $^3J_{HH}$ = 7.6 Hz,), 6.75 (dd, 4H, *o*,*m*-Ar, $^3J_{HH}$ = 7.6, 2.3 Hz), 5.58 (s, 1H, *H*C(C(Me)NAr)$_2$), 3.88−3.84 (sept, 2H, C*H*Me$_2$, $^3J_{HH}$ = 5.0 Hz), 3.42−3.37 (sept, 2H, C*H*Me$_2$, $^3J_{HH}$ = 5.0 Hz), 1.83 (s, 6H, HC(C(*Me*)NAr)$_2$), 1.42 (s, 9H, N^t*Bu*), 1.08 (d, 6H, CH*Me*$_2$, $^3J_{HH}$ = 5.0 Hz), 1.02 (d, 6H, CH*Me*$_2$, $^3J_{HH}$ = 5.0 Hz), 0.91 (d, 6H, CH*Me*$_2$, $^3J_{HH}$ = 5.0 Hz), 0.32 (d, 6H, CH*Me*$_2$, $^3J_{HH}$ = 5.01 Hz). $^{13}C\{^1H\}$ NMR (125.8 MHz, $CDCl_3$, 293 K): δ = 171.18 (C, HC(*C*(Me)NAr)$_2$), 155.23 (C, Ar), 142.58 (C, Ar), 141.24 (C, Ar), 125.79 (CH, Ar), 125.01 (CH, Ar), 123.42 (CH, Ar), 105.68 (CH, HC(C(Me)NAr)$_2$), 66.73 (C(Me)$_3$), 33.78 (CH$_3$, Nb═N^t*Bu*), 28.55 (CH, ^{i}Pr), 27.54 (CH, ^{i}Pr), 25.99 (CH$_3$, HC(C(*Me*)NAr)$_2$), 25.53 (CH$_3$, ^{i}Pr), 25.44 (CH$_3$, ^{i}Pr), 25.20 (CH$_3$, ^{i}Pr), 23.96 (CH$_3$, ^{i}Pr). FT-IR (cm^{-1}): 2934 (w), 2881(w), 1518 (m), 1434 (m), 1381 (m), 1361 (m), 1312 (m), 1248 (s), 1169 (w), 1107 (w), 1012 (m), 934 (m), 851 (s), 794 (s), 776 (m), 756 (m), 680 (m). UV−vis (toluene): λ_1 = 317 nm (ε = 36 000 L·cm^{-1}·mol^{-1}); λ_2 = 603 nm (ε = 30 000 L·cm^{-1}·mol^{-1}). ES-MS: *m*/*z* = 1462.5900 [M]$^+$ (calcd for $C_{66}H_{100}N_6P_4Ta_2$: 1462.5926). Anal. Calcd for $C_{66}H_{100}F_{40}N_6Ta_2P_4$: C, 54.17; H, 6.89; N, 5.74. Found: C, 53.86; H, 6.62; N, 5.91. mp: (decomp) 344−346 °C.

{[(BDI$^{\#}$)Nb(N^{t}Bu)]$_2$(μ-η^3:η^{3}P$_4$)}[B(C$_6$F$_5$)$_4$]$_2$ ***(4)***. [HOEt$_2$][B(C$_6$F$_5$)$_4$] (117 mg, 0.155 mmol, 2 equiv) was added to an 8 mL α,α,α-trifluorotoluene suspension of **1** (100 mg, 0.078 mmol, 1 equiv). The reaction mixture was stirred for 1 h at room temperature and turned from turquoise green to dark green. The mixture was then filtered to give a green filtrate that was cooled at −40 °C and left standing overnight in the freezer. This afforded pink crystals that were recovered, washed with 2 × 1 mL of Et$_2$O, and dried *in vacuo* to give **4** as a pink crystalline material (168 mg, 0.064 mmol, 82%). Single crystals suitable for X-ray diffraction were obtained similarly. ^1H NMR (400 MHz, $C_2H_4Cl_2$:$CDCl_3$ 95:5, 293 K): δ = 7.05 (t, 4H, C*H*$_{Ar}$, $^3J_{HH}$ = 7.9 Hz), 6.90 (d, 4H, C*H*$_{Ar}$, $^3J_{HH}$ = 8.0 Hz), 6.79 (d, 4H, C*H*$_{Ar}$, $^3J_{HH}$ = 7.9 Hz), 5.44 (d, 2H, *H*$_2$C(C(Me)NAr)$_2$, $^2J_{HH}$ = 16.7 Hz), 4.68 (d, 2H, *H*$_2$C(C(Me)NAr)$_2$, $^2J_{HH}$ = 16.7 Hz), 2.80 (sept, 4H, C*H*Me$_2$, $^3J_{HH}$ = 6.6 Hz), 2.71 (sept, 4H, C*H*Me$_2$, $^3J_{HH}$ = 6.6 Hz), 2.29 (s, 12H, HC(C(*Me*)NAr)$_2$), 1.57 (s, 18H, N^t*Bu*), 1.00 (dd, 24H, CHMe*Me*, $^3J_{HH}$ = 6.6 Hz), 0.93 (d, 12H, CHMe*Me*, $^3J_{HH}$ = 6.6 Hz), 0.36 (d, 12H, CHMe*Me*, $^3J_{HH}$ = 6.6 Hz). ^{19}F NMR (376 MHz, THF-d_8, 293 K): δ = −132.1, −162.6, and −166.5 (B(C$_6$F$_5$)$_4$). FT-IR (cm^{-1}): 2970 (w), 2847 (w), 1643 (w), 1620 (w), 1513 (m), 1455 (s), 1372 (m), 1322 (m), 1273 (m), 1204 (m), 1172 (m), 1132 (m), 1086 (s), 975 (s), 933 (w), 842 (w), 798 (m), 773 (m), 755 (m), 702 (m), 683 (m), 659 (m). UV−vis ($C_2H_4Cl_2$): λ_1 = 694 nm (ε = 29 900 L·cm^{-1}·mol^{-1}), λ_2 = 515 nm (ε = 4250 L·cm^{-1}·mol^{-1}), λ_3 = 325 nm (ε = 19 900 L·cm^{-1}·mol^{-1}). Anal. Calcd for $C_{114}H_{102}F_{40}B_2N_6Nb_2P_4$: C, 51.72; H, 3.88; N, 3.17. Found: C, 51.56; H, 3.94; N, 3.11. mp: 221−223 °C.

{[(BDI)Nb(N^{t}Bu)]$_2$(μ-η^3:η^{3}P$_4$)}[B(C$_6$F$_5$)$_4$] ***(5)***. A 3 mL THF solution of AgB(C$_6$F$_5$)$_4$ (122 mg, 0.155 mmol, 1 equiv) was added to a 20 mL toluene solution of **1** (200 mg, 0.155 mmol, 1 equiv). The reaction mixture was stirred for 1 h at room temperature. The solids were recovered by filtration, washed with 1 mL of toluene, and extracted with 3 × 2 mL of α,α,α-trifluorotoluene. The dark green suspension was filtered, layered with 12 mL of *n*-hexane, and left standing at room temperature for 3 days. This gave dark green crystals of **5** that were recovered, washed with *n*-hexane, and dried *in vacuo* (236 mg, 0.120 mmol, 77%). Dark green block-shaped single crystals suitable for X-ray diffraction were obtained similarly. The ^1H NMR spectrum (600 MHz, $CDCl_3$, 223 to 333 K) recorded for this paramagnetic radical species features uninformative broad signals in the −0.5 to +8.9 ppm range. FT-IR (cm^{-1}): 2970 (w), 2882 (w), 1643 (w), 1514 (m), 1455 (s), 1352 (m), 1315 (m), 1258 (m), 1210 (m), 1178 (w), 1125 (w), 1085 (s), 1022 (w), 978 (s), 932 (m), 856 (s), 795 (s), 771 (s), 755 (s), 697 (m), 683 (m), 659 (m). UV−vis ($CF_3C_6H_5$): λ_1 = 921 nm (ε = 22 750 L·cm^{-1}·mol^{-1}), λ_2 = 655 nm (ε = 7060 L·cm^{-1}·mol^{-1}), λ_3 = 435 nm (ε = 7100 L·cm^{-1}·mol^{-1}), λ_4 = 372 nm (ε = 17 600 L·cm^{-1}·mol^{-1}), λ_5 = 330 nm (ε = 31 500 L·cm^{-1}·mol^{-1}), λ_6 = 296 nm (ε = 35 300 L·cm^{-1}·mol^{-1}). ES-MS: *m*/*z* = 1286.5074 [[(BDI)Nb(N^{t}Bu)]$_2$(μ-η^3:η^{3}P$_4$)]$^+$ (calcd for $C_{66}H_{100}N_6Nb_2P_4$: 1286.5093). Anal. Calcd for $C_{90}H_{100}F_{20}BN_6Nb_2P_4$: C, 54.98; H, 5.13; N, 4.27. Found: C, 55.08; H, 5.43; N, 4.06. mp: (decomp) 279−281 °C.

{[(BDI)Nb(N^{t}Bu)]$_2$(μ-η^3:η^{3}P$_4$)}[B(C$_6$F$_5$)$_4$]$_2$ ***(6)***. A 2 mL THF solution of AgB(C$_6$F$_5$)$_4$ (92 mg, 0.117 mmol, 3 equiv) was added to a 20 mL toluene solution of **1** (50 mg, 0.039 mmol, 1 equiv). The reaction mixture was stirred for 1 h at room temperature. The solids were recovered by filtration, washed with 1 mL of toluene, and extracted with 24 mL of α,α,α-trifluorotoluene. The dark purple suspension was filtered, layered with 50 mL of *n*-hexane, and left standing at room temperature for 2 days. This produced dark purple needle-shaped crystals of **6** that were recovered, washed with *n*-hexane, and dried *in vacuo* (66 mg, 0.025 mmol, 64%). Dark purple needle-shaped single crystals suitable for X-ray diffraction were obtained similarly. ^1H NMR (600 MHz, $CF_3C_6H_5$:C_6D_6 95:5, 293 K): *resonances of aromatic protons could not be detected because of overlap with solvent*, δ = 6.90 (s, 2H, *H*C(C(Me)NAr)$_2$), 2.96−2.88 (sept, 4H, C*H*Me$_2$, $^3J_{HH}$ = 6.6 Hz), 2.68−2.61 (sept, 4H, C*H*Me$_2$, $^3J_{HH}$ = 6.6 Hz), 2.18 (s, 12H, HC(C(*Me*)NAr)$_2$), 1.26 (s, 18H, N^t*Bu*), 1.10 (d, 24H, CHMe*Me*, $^3J_{HH}$ = 6.5 Hz), 1.05 (d, 12H, CHMe*Me*, $^3J_{HH}$ = 6.6 Hz), 0.62 (d, 12H, CHMe*Me*, $^3J_{HH}$ = 6.6 Hz). ^{19}F NMR (376 MHz, $CF_3C_6H_5$:C_6D_6 95:5, 293 K): δ = −131.4, −162.8, and −166.5 (B(C$_6$F$_5$)$_4$). ^{31}P NMR (243 MHz, $CF_3C_6H_5$:C_6D_6 95:5, 293 K): δ = 516 (s, P_4). FT-IR (cm^{-1}): 2971 (w), 2862 (w), 1644 (w), 1513 (m), 1456 (s), 1373 (m), 1321 (m), 1272 (m), 1203 (m), 1174 (m), 1132 (m), 1085 (s), 976 (s), 931 (m), 801 (m), 773 (m), 755 (m), 702 (m), 683 (m), 659 (m). UV−vis

dx.doi.org/10.1021/ja5107282 | J. Am. Chem. Soc. 2014, 136, 17652−17661

($CF_3C_6H_5$): λ_1 = 527 nm (ε = 6150 L·cm^{-1}·mol^{-1}), λ_2 = 325 nm (ε = 21 350 L·cm^{-1}·mol^{-1}). Anal. Calcd for $C_{114}H_{100}F_{40}B_2N_6Nb_2P_4$: C, 51.76; H, 3.81; N, 3.18. Found: C, 51.77; H, 3.70; N, 3.12. mp: (decomp) 229−232 °C.

*Reduction of **5** into **1**.* A 0.5 mL α,α,α-trifluorotoluene solution of $CoCp_2$ (1.4 mg, 0.008 mmol, 1 equiv) was added to a 4 mL α,α,α-trifluorotoluene solution of **5** (15 mg, 0.008 mmol, 1 equiv). The reaction was stirred for 1 h at room temperature, and the color turned from dark green to turquoise green. The solvent was removed *in vacuo*, the residue was extracted with $CDCl_3$, and the green solution was analyzed by ^{1}H NMR, showing the characteristic resonances for **1**.

*[(BDI)Nb(N^{t}Bu)(OTf)$_2$] (**7**).* A 2 mL toluene solution of AgOTf (40 mg, 0.155 mmol, 2 equiv) was added to an 8 mL toluene solution of **1** (100 mg, 0.078 mmol, 1 equiv). The reaction mixture was stirred overnight at room temperature before filtration. The resulting pale, bright lime green solution was concentrated and stored at −40 °C overnight. This produced yellow crystals of **7** that were collected and dried *in vacuo* (33.0 mg, 0.038 mmol, 24%). Single crystals suitable for X-ray diffraction were grown similarly. ^{1}H NMR (500 MHz, C_6D_6, 293 K): δ = 7.03 (m, 4H, C−H$_{Ar}$), 6.94 (m, 2H, C−H$_{Ar}$), 6.24 (s, 1H, HC(C(Me)NAr)$_2$), 2.59−2.48 (m, 4H, CHMe$_2$), 1.90 (s, 6H, HC(C(Me)NAr)$_2$), 1.66 (d, 6H, CHMe$_2$, $^3J_{HH}$ = 6.4 Hz), 1.28 (d, 6H, CHMe$_2$, $^3J_{HH}$ = 6.4 Hz), 1.07 (d, 6H, CHMe$_2$, $^3J_{HH}$ = 6.7 Hz), 0.83 (d, 6H, CHMe$_2$, $^3J_{HH}$ = 6.7 Hz), 0.75 (s, 9H, N^{t}Bu). ^{13}C{^{1}H} NMR (125.8 MHz, C_6D_6, 293 K): δ = 173.53 (C, HC(C(Me)NAr)$_2$), 144.83 (C, Ar), 144.28 (C, Ar), 139.93 (C, Ar), 129.19 (CH, Ar), 125.07 (CH, Ar), 125.04 (CH, Ar), 113.69 (CH, HC(C(Me)NAr)$_2$), 69.89 (C(Me)$_3$), 33.89 (CH, ^{i}Pr), 30.26 (CH$_3$, Nb=N^{t}Bu), 28.32 (CH, ^{i}Pr), 26.13 (CH$_3$, HC(C(Me)NAr)$_2$), 25.67 (CH$_3$, ^{i}Pr), 24.99 (CH$_3$, ^{i}Pr), 24.85 (CH$_3$, ^{i}Pr), 24.71 (CH$_3$, ^{i}Pr). ^{19}F NMR (376 MHz, C_6D_6, 293 K): δ = −75.37 (q, 3F, CF$_3$, J_{FF} = 4.9 Hz), −77.12 ppm (q, 3F, CF$_3$, J_{FF} = 4.9 Hz). FT-IR (cm^{-1}): 2970 (w), 2936 (w), 2874 (w), 1532 (w), 1462 (w), 1432 (w), 1372 (w), 1335 (m), 1231 (m), 1187 (s), 1173 (s), 1020 (s), 987 (s), 932 (m), 887 (w), 852 (w), 801 (m), 759 (w), 731 (m), 631 (s), 566 (m). Anal. Calcd for $C_{35}H_{50}F_6N_3NbO_6S_2$ C, 47.78 ; H, 5.73 ; N, 4.78. Found: C, 47.75 ; H, 5.79; N, 4.67. mp: (decomp) 258−260 °C.

■ ASSOCIATED CONTENT

Supporting Information

NMR, IR, and ESI-MS spectra; X-ray crystallography structural details and files in CIF format; and computational data. This material is available free of charge via the Internet at http://pubs.acs.org.

■ AUTHOR INFORMATION

Corresponding Authors

laurent.maron@irsamc.ups-tlse.fr
rbergman@berkeley.edu
arnold@berkeley.edu

Notes

The authors declare no competing financial interest.

■ ACKNOWLEDGMENTS

We thank the AFOSR (Grant No. FA9550-11-1-0008) for funding and NIH shared instrumentation grant S10-RR027172. We thank N. Settineri, A. DiPascuale, R. Chatterjee, W. W. Luckens, C. Canlas, and Z. Zhongrui for experimental assistance and B. Kriegel and T. L. Gianetti for helpful discussions.

■ REFERENCES

(1) Bachhuber, F.; von Appen, J.; Dronskowski, R.; Schmidt, P.; Nilges, T.; Pfitzner, A.; Weihrich, R. *Angew. Chem., Int. Ed.* **2014**, *53*, 11629.

(2) Cotton, F. A.; Wilkinson, G.; Murillo, C. A.; Bochmann, M. *Advanced Inorganic Chemistry*, 6th ed.; John Wiley & Sons: New York, 1999.

(3) Scheer, M.; Balázs, G.; Seitz, A. *Chem. Rev.* **2010**, *110*, 4236.

(4) Cossairt, B. M.; Piro, N. A.; Cummins, C. C. *Chem. Rev.* **2010**, *110*, 4164.

(5) Urnius, E.; Brennessel, W. W.; Cramer, C. J.; Ellis, J. E.; Schleyer, P. v. R. *Science* **2002**, *295*, 832.

(6) Laplaza, C. E.; Davis, W. M.; Cummins, C. C. *Angew. Chem., Int. Ed. Engl.* **1995**, *34*, 2042.

(7) Cossairt, B. M.; Diawara, M.-C.; Cummins, C. C. *Science* **2009**, *323*, 602.

(8) Seidel, W. W.; Summerscales, O. T.; Patrick, B. O.; Fryzuk, M. D. *Angew. Chem., Int. Ed.* **2009**, *48*, 115.

(9) Peng, Y.; Fan, H.; Zhu, H.; Roesky, H. W.; Magull, J.; Hughes, C. E. *Angew. Chem., Int. Ed.* **2004**, *43*, 3443.

(10) Schwarzmaier, C.; Noor, A.; Glatz, G.; Zabel, M.; Timoshkin, A. Y.; Cossairt, B. M.; Cummins, C. C.; Kempe, R.; Scheer, M. *Angew. Chem., Int. Ed.* **2011**, *50*, 7283.

(11) Heinl, S.; Scheer, M. *Chem. Sci.* **2014**, *5*, 3221.

(12) Demange, M.; Le Goff, X.-F.; Le Floch, P.; Mézailles, N. *Chem.—Eur. J.* **2010**, *16*, 12064.

(13) Dürr, S.; Ertler, D.; Radius, U. *Inorg. Chem.* **2012**, *51*, 3904.

(14) Pelties, S.; Herrmann, D.; de Bruin, B.; Hartl, F.; Wolf, R. *Chem. Commun.* **2014**, *50*, 7014.

(15) Caporali, M.; Gonsalvi, L.; Mirabello, V.; Ienco, A.; Manca, G.; Zanobini, F.; Peruzzini, M. *Eur. J. Inorg. Chem.* **2014**, *2014*, 1652.

(16) Konchenko, S. N.; Pushkarevsky, N. a; Gamer, M. T.; Köppe, R.; Schnöckel, H.; Roesky, P. W. *J. Am. Chem. Soc.* **2009**, *131*, 5740.

(17) Tran, B. L.; Singhal, M.; Park, H.; Lam, O. P.; Pink, M.; Krzystek, J.; Ozarowski, A.; Telser, J.; Meyer, K.; Mindiola, D. J. *Angew. Chem., Int. Ed.* **2010**, *49*, 9871.

(18) Caporali, M.; Gonsalvi, L.; Rossin, A.; Peruzzini, M. *Chem. Rev.* **2010**, *110*, 4178.

(19) Peruzzini, M.; Gonsalvi, L.; Romerosa, A. *Chem. Soc. Rev.* **2005**, *34*, 1038.

(20) Li, T.; Kaercher, S.; Roesky, P. W. *Chem. Soc. Rev.* **2014**, *43*, 42.

(21) Piro, N.; Figueroa, J. S.; McKellar, J. T.; Cummins, C. C. *Science* **2006**, *313*, 1276.

(22) Cossairt, B. M.; Cummins, C. C. *Angew. Chem., Int. Ed.* **2010**, *49*, 1595.

(23) Figueroa, J. S.; Cummins, C. C. *J. Am. Chem. Soc.* **2004**, *126*, 13916.

(24) Heinl, S.; Reisinger, S.; Schwarzmaier, C.; Bodensteiner, M.; Scheer, M. *Angew. Chem., Int. Ed.* **2014**, *53*, 7639.

(25) Mädl, E.; Butovskii, M. V.; Balázs, G.; Peresypkina, E. V.; Virovets, A. V.; Seidl, M.; Scheer, M. *Angew. Chem., Int. Ed.* **2014**, *53*, 7643.

(26) Mirabello, V.; Caporali, M.; Gonsalvi, L.; Manca, G.; Ienco, A.; Peruzzini, M. *Chem.—Asian J.* **2013**, *8*, 3177.

(27) Barbaro, P.; Di Vaira, M.; Peruzzini, M.; Seniori Costantini, S.; Stoppioni, P. *Angew. Chem., Int. Ed.* **2008**, *47*, 4425.

(28) Barbaro, P.; Bazzicalupi, C.; Peruzzini, M.; Seniori Costantini, S.; Stoppioni, P. *Angew. Chem., Int. Ed.* **2012**, *51*, 8628.

(29) Scheer, M.; Herrmann, E.; Joachim, S.; Matthias, O. *Angew. Chem., Int. Ed. Engl.* **1991**, *103*, 969.

(30) Scherer, O. J.; Vondung, J.; Wolmershäuser, G. *Angew. Chem., Int. Ed. Engl.* **1989**, *28*, 1355.

(31) Scheer, M.; Troitzsch, C.; Jones, P. G. *Angew. Chem., Int. Ed. Engl.* **1992**, *31*, 1377.

(32) Frey, A. S. P.; Cloke, F. G. N.; Hitchcock, P. B.; Green, J. C. *New J. Chem.* **2011**, *35*, 2022.

(33) Stephens, F. H. Activation of White Phosphorus by Molybdenum and Uranium tris-Amides. Ph.D. Thesis, Massachussets Institute of Technology, 2004.

(34) Kraus, F.; Hanauer, T.; Korber, N. *Inorg. Chem.* **2006**, *45*, 1117.

(35) Kraus, F.; Aschenbrenner, J. C.; Korber, N. *Angew. Chem., Int. Ed.* **2003**, *42*, 4030.

(36) Velian, A.; Cummins, C. *Chem. Sci.* **2012**, *3*, 1003.

(37) Smith, R. C.; Urnezius, E.; Lam, K.-C.; Rheingold, A. L.; Protasiewicz, J. D. *Inorg. Chem.* **2002**, *41*, 5296.
(38) Niecke, E.; Rüger, R.; Krebs, B. *Angew. Chem., Int. Ed. Engl.* **1982**, *21*, 544.
(39) He, G.; Shynkaruk, O.; Lui, M. W.; Rivard, E. *Chem. Rev.* **2014**, *114*, 7815.
(40) Tomson, N. C.; Arnold, J.; Bergman, R. G. *Organometallics* **2010**, *29*, 5010.
(41) Kriegel, B. M.; Bergman, R. G.; Arnold, J. *Dalton Trans.* **2014**, *43*, 10046.
(42) Gianetti, T. L.; Tomson, N. C.; Arnold, J.; Bergman, R. G. *J. Am. Chem. Soc.* **2011**, *133*, 14904.
(43) Gianetti, T. L.; Bergman, R. G.; Arnold, J. *Chem. Sci.* **2014**, *5*, 2517.
(44) Gianetti, T. L.; Bergman, R. G.; Arnold, J. *J. Am. Chem. Soc.* **2013**, *135*, 8145.
(45) Gianetti, T. L.; Nocton, G.; Minasian, S. G.; Tomson, N. C.; Kilcoyne, a L. D.; Kozimor, S. A; Shuh, D. K.; Tyliszczak, T.; Bergman, R. G.; Arnold, J. *J. Am. Chem. Soc.* **2013**, *135*, 3224.
(46) Obenhuber, A. H.; Gianetti, T. L.; Berrebi, X.; Bergman, R. G.; Arnold, J. *J. Am. Chem. Soc.* **2014**, *136*, 2994.
(47) Tomson, N. C.; Arnold, J.; Bergman, R. G. *Organometallics* **2010**, *29*, 2926.
(48) Hönle, W.; Von Schnering, H. G.; Schmidpeter, A.; Burget, G. *Angew. Chem., Int. Ed. Engl.* **1984**, *23*, 817.
(49) Patel, D.; Tuna, F.; McInnes, E. J. L.; Lewis, W.; Blake, A. J.; Liddle, S. T. *Angew. Chem., Int. Ed.* **2013**, *52*, 13334.
(50) Huang, W.; Diaconescu, P. L. *Chem. Commun.* **2012**, *48*, 2216.
(51) Scharfe, S.; Kraus, F.; Stegmaier, S.; Schier, A.; Fässler, T. F. *Angew. Chem., Int. Ed.* **2011**, *50*, 3630.
(52) Böcker, S.; Häser, M. *Z. Anorg. Allg. Chem.* **1995**, *621*, 258.
(53) Von Schnering, H. G.; Hönle, W. *Chem. Rev.* **1988**, *88*, 243.
(54) Von Schnering, H. G. *Angew. Chem., Int. Ed. Engl.* **1981**, *20*, 33.
(55) Masuda, J. D.; Schoeller, W. W.; Donnadieu, B.; Bertrand, G. *J. Am. Chem. Soc.* **2007**, *129*, 14180.
(56) Scherer, O.; Berg, G.; Wolmershäuser, G. *Chem. Ber.* **1996**, *129*, 53.
(57) Gianetti, T. L.; Nocton, G.; Minasian, S. G.; Kaltsoyannis, N.; Kilcoyne, A. L. D.; Kozimor, S.; Shuh, D. K.; Tyliszczak, T.; Bergman, R. G.; Arnold, J. *Chem. Sci.* **2014**, DOI: 10.1039/C4SC02705A.
(58) Camp, C.; Arnold, J. Manuscript submitted.
(59) Duling, D. R. *J. Magn. Reson. Ser. B* **1994**, *104*, 105.